New Journal of Physics
The open-access journal for physics

Effective three-body interactions of neutral bosons in optical lattices

P R Johnson[1,2,3], E Tiesinga[2], J V Porto[2] and C J Williams[2]

[1] Department of Physics, American University, Washington, DC 20016, USA
[2] Joint Quantum Institute, National Institute of Standards and Technology and University of Maryland, Gaithersburg, MD 20899, USA
E-mail: pjohnson@american.edu

New Journal of Physics **11** (2009) 093022 (14pp)
Received 16 June 2009
Published 15 September 2009
Online at http://www.njp.org/
doi:10.1088/1367-2630/11/9/093022

Abstract. We show that there are *effective* three- and higher-body interactions generated by the two-body collisions of atoms confined in the lowest vibrational states of a three-dimensional (3D) optical lattice. The collapse and revival dynamics of approximate coherent states loaded into a lattice are a particularly sensitive probe of these higher-body interactions; the visibility of interference fringes depend on both two-, three- and higher-body energy scales, and these produce an initial dephasing that can help explain the surprisingly rapid decay of revivals seen in experiments. If inhomogeneities in the lattice system are sufficiently reduced, longer timescale partial and nearly full revivals will be visible. Using Feshbach resonances or control of the lattice potential it is possible to tune the effective higher-body interactions and simulate effective field theories in optical lattices.

[3] Author to whom any correspondence should be addressed.

Contents

1. Introduction

The collapse and revival of matter-wave coherence is an expected consequence of two-body atom–atom interactions in trapped Bose–Einstein condensates (BECs) [1]–[4]. Collapse and revival of few-atom coherent states in optical lattices has been seen in a number of experiments, first in single-well lattices [5] and subsequently in double-well lattices [6, 7][4]. In these experiments, a BEC is quickly loaded into a fairly deep three-dimensional (3D) lattice such that the quantum state approximately factors into a product of coherent states localized to each lattice site [8]–[10]. Each coherent state, which is a superposition of different atom-number states, initially has a well-defined phase. If the lattice potential is quickly turned off before atom–atom interactions have a significant influence, the coherent states released from confinement at each site expand and overlap resulting in interference fringes in the imaged atom-density. However, if the atoms are held in the lattice for a longer duration before release, interactions will play a significant role by causing the phases of the different atom-number states in the superposition at each site to evolve at different rates. This will result in a dephasing of the coherent state, and a subsequent collapse of the interference fringe visibility after the atoms are released. For atoms in a homogeneous lattice with two-body interactions and negligible tunneling, the coherent states at each lattice site are predicted to revive when the atom-number component states simultaneously re-phase after multiples of the time $t_2 = 2\pi\hbar/U_2$, where U_2 is the two-body interaction energy [1]–[5].

In addition to the expected two-body physics described above, we show that the data in [5]–[7] should also contain strong signatures of *coherent* three- and higher-body interactions. In contrast to the coherent dynamics described in this paper, recent experiments have studied inelastic three-body processes, including recent observations of Efimov physics [11]–[13], by tracking atom loss from recombination [14]. There has been a growing interest in three- and four-body physics (e.g. [15]–[20]), and the role of intrinsic three-body interactions on equilibrium quantum phases in optical lattices has been studied in [21]–[23]. The influence of higher bands on the Mott-insulator phase transition has been analyzed in [24], and three-body interactions of fermions and polar molecules in lattices have also been explored [25].

In this paper, we use the ideas of effective field theory to show that virtual transitions to higher vibrational states generate *effective*, coherent three-body interactions between atoms in the lowest vibrational states of a deep 3D lattice where tunneling can be neglected. More

[4] These experiments focused on binomially split number states, but also included experiments on coherent states.

generally, virtual excitations also generate effective four- and higher-body interactions giving the non-equilibrium dynamics multiple energy scales. We also show that loading coherent states into an optical lattice creates a sensitive interferometer for probing higher-body interactions. In a sufficiently uniform lattice, multiple frequencies manifested as beatings in the visibility of the collapse and revival oscillations give a direct method for measuring the energy and frequency scales for elastic higher-body interactions. Remarkably, multiple-frequency collapse and revival patterns have been seen in recent experiments [26].

Three-body interactions can also explain the surprisingly rapid damping of revivals seen in [5]–[7], where the overall visibility of the interference fringes decays after roughly five revivals ($\sim$3 ms for the system parameters in [5]–[7]). This short timescale cannot be explained in terms of tunneling or atom loss. For example, for the system parameters in [5]–[7], the tunneling-induced decoherence timescale has been found to be a factor of 10–100 times too long [27], and the atom loss from three-body recombination [14] appears to be negligible [26]. The latter observation is consistent with the expected three-body recombination timescales for ^{87}Rb in a lattice[5].

The damping of revivals can be partially explained by the expected variation in U_2 over a non-uniform lattice due to an additional harmonic term in the trapping potential. Inhomogeneity in U_2 causes dephasing due to the variation in the revival times for coherent states at different sites; however, the estimated 3–5% inhomogeneity of U_2 should allow as many as 10–20 revivals compared to the $\sim$5 seen in [5]–[7]. In contrast, we show below that coherent three-body interactions can cause dephasing of coherent states at each lattice site after only a few revivals.

The effective theory in this paper describes the low-energy, small scattering length, small atom number per lattice site regime, for deep 3D lattices with negligible tunneling. These approximations are reasonable for the experiments in [5]–[7]. Extensions of the analysis might include tunneling, including second-order [28] and interaction-driven [29] tunneling, and the incorporation of intrinsic higher-body interactions. Effective field theory has also proven to be an important tool in the large scattering length limit [12]. It would be particularly interesting to simulate the controlled breakdown of the effective theory developed here by increasing the scattering length or atom number, or by tuning other lattice parameters. Looking beyond the realm of atomic physics, our analysis suggests interesting possibilities for using optical lattices to test important mechanisms in effective field theory [30].

In section 2, we construct a multimode Hamiltonian $\hat{H}$ that we use to obtain an effective single-mode Hamiltonian $\tilde{H}_{\rm eff}$. In section 3, we describe the physical processes that generate higher-body interactions. In section 4, we estimate the effective three-body energy. In section 5, we show how the coherent three-body interactions modify the collapse and revival dynamics. Finally, we summarize our results in section 6.

2. Effective three-body model for neutral bosons in an optical lattice

A many-body Hamiltonian for mass m_a neutral bosons in a single spin state can be written as

$$\mathcal{H} = \int \hat{\psi}^\dagger H_0 \hat{\psi}\, \mathrm{d}\mathbf{r} + \tfrac{1}{2}\int \hat{\psi}^\dagger(\mathbf{r})\hat{\psi}^\dagger(\mathbf{r}')V_2(\mathbf{r},\mathbf{r}')\hat{\psi}(\mathbf{r})\hat{\psi}(\mathbf{r}')\,\mathrm{d}\mathbf{r}\mathrm{d}\mathbf{r}' + \tfrac{1}{6}\int \hat{\psi}^\dagger(\mathbf{r})\hat{\psi}^\dagger(\mathbf{r}')\hat{\psi}^\dagger(\mathbf{r}'')V_3(\mathbf{r},\mathbf{r}',\mathbf{r}'')\hat{\psi}(\mathbf{r})\hat{\psi}(\mathbf{r}')\hat{\psi}(\mathbf{r}'')\,\mathrm{d}\mathbf{r}\mathrm{d}\mathbf{r}'\mathrm{d}\mathbf{r}'' + \cdots, \quad (1)$$

[5] Using the three-body loss rate $\simeq 6\times10^{-30}\,\mathrm{cm}^6\,\mathrm{s}^{-1}$, the loss rate for n atoms in a 40 kHz lattice site is $2.5n^2\,\mathrm{s}^{-1}$ and the lifetime for $n=3$ atoms is $\gtrsim 60$ ms.

where V_m are intrinsic m-body interaction potentials, and H_0 is the Hamiltonian for a single particle in the optical lattice. We set $V_{m>2} = 0$ to focus on the physics of effective interactions induced by V_2. In experiments, the effect of intrinsic and effective interactions are both present.

It is our goal to construct a low energy, effective Hamiltonian $\tilde{H}_{\text{eff}}$ for describing a small number of atoms in the vibrational ground state of a lattice site, while incorporating leading-order corrections from virtual excitation to higher bands. In the quantum mechanical approach, Huang *et al* [31] have shown that a local regularized delta-function potential $V_2(\mathbf{r}, \mathbf{r}') \propto \delta^{(3)}(\mathbf{r} - \mathbf{r}')(\mathrm{d}/\mathrm{d}\varrho)\varrho$, where $\varrho = |\mathbf{r} - \mathbf{r}'|$, can be used to obtain the low-energy scattering for two particles. To go beyond the two-particle case, we find it convenient to instead use the renormalization methods of quantum field theory and the non-regularized delta-function potential

$$V_2(\mathbf{r}, \mathbf{r}') = g_2 \delta^{(3)}(\mathbf{r} - \mathbf{r}'). \tag{2}$$

We regularize the theory in perturbation theory by using a high-energy cutoff Λ in the sum over intermediate states, which is equivalent to using a regularized (non-singular) potential. We view Λ as a physical threshold beyond which the low-energy theory fails. We note that the low-energy physics does not, in the end, depend on the method of regularization, and that the physical results found below after renormalization are insensitive to Λ. The key observation is that even if a fully regularized form of V_2 is used renormalization is still required recognizing that the *bare* parameter g_2 is not the physical (renormalized) coupling strength $\tilde{g}_2$. (In the following, we use a tilde to distinguish between bare and renormalized parameters.)

Employing renormalized perturbation theory [30], we write $g_2 = \tilde{g}_2 + c$, where

$$\tilde{g}_2 = \frac{4\pi\hbar^2 a_{\text{scat}}}{m_a} + \mathcal{O}(a_{\text{scat}}^2) \tag{3}$$

is chosen to reproduce the exact, low-energy limit given in [32] for two atoms in a spherically symmetric harmonic trap, and a_{scat} is the scattering length at zero-collisional energy. The first-order approximation to $\tilde{g}_2$ suffices for the calculation of the three-body energy at second order given below. The value of the counter-term c, which cancels the contributions to the two-body interaction energy that diverge with Λ, is determined by the normalization condition equation (3). The local Hamiltonian with counter-term and physical coupling parameter becomes

$$\mathcal{H} = \int \hat{\psi}^\dagger H_0 \hat{\psi}\, \mathrm{d}\mathbf{r} + \tfrac{1}{2}(\tilde{g}_2 + c) \int \hat{\psi}^\dagger \hat{\psi}^\dagger \hat{\psi}\hat{\psi}\, \mathrm{d}\mathbf{r}. \tag{4}$$

To develop a low-energy effective theory for a deep optical lattice, we expand the field over a set of bosonic annihilation operators $\hat{a}_{i\mu}$ and single particle wavefunctions $\phi_{i\mu}(\mathbf{r})$ giving $\hat{\psi}(\mathbf{r}) = \sum_{i\mu} \phi_{i\mu}(\mathbf{r})\hat{a}_{i\mu}$, where the indices $\mu = \{\mu_x, \mu_y, \mu_z\}$ with $\mu_{x,y,z} = 0, 1, 2, \ldots$ label 3D vibrational states and i labels the lattice sites. To focus on the role of interactions we assume a deep lattice with $n_s \gtrsim 3$ states per spatial dimension at each site, making tunneling of atoms in the ground vibrational state $\mu = \{0, 0, 0\} \equiv 0$ negligible on the timescale of interest [5]. Since we are not considering the role of tunneling, for simplicity we use isotropic harmonic oscillator wavefunctions at each site with frequency ω and length scale $\sigma = \sqrt{\hbar/m_a\omega}$ determined by the (approximately) harmonic confinement within a single lattice well. Note that even with tunneling neglected, anharmonicity of the lattice potential is a potentially significant effect. We also expect our model to break down or to require significant modification for very

shallow lattices or near the Mott-insulator phase transition where the effects of tunneling are important [24], [33]–[35].

Inserting the expansion for $\hat{\psi}$ into $\mathcal{H}$, interchanging the order of integration over $\mathbf{r}$ and summation over modes, and dropping terms that transfer atoms between sites (e.g. tunneling), we obtain for each lattice site the multimode Hamiltonian $\hat{H} = \hat{H}_0 + \hat{H}_2$, where

$$\hat{H}_0 = \sum_{\mu} E_\mu \hat{a}_\mu^\dagger \hat{a}_\mu \tag{5}$$

and

$$\hat{H}_2 = \tfrac{1}{2}(\tilde{U}_2 + A) \sum_{\mu\nu\sigma\lambda} K_{\mu\nu\sigma\lambda} \hat{a}_\mu^\dagger \hat{a}_\nu^\dagger \hat{a}_\sigma \hat{a}_\lambda. \tag{6}$$

For brevity we suppress the lattice site index i. The single-particle energies are $E_\mu = (\mu_x + \mu_y + \mu_z)\hbar\omega$, setting the ground-state energy $E_0 \equiv E_{\{0,0,0\}} = 0$. The two-body interaction energy for ground state atoms is

$$\tilde{U}_2 = \frac{\tilde{g}_p}{(2\pi)^{3/2}\sigma^3} = \sqrt{\frac{2}{\pi}}\hbar\omega(a_{\mathrm{scat}}/\sigma), \tag{7}$$

and $A = (2\pi)^{-3/2}c/\sigma^3$ is the counter-term in units of energy. The matrix elements

$$K_{\mu\nu\gamma\delta} = (2\pi)^{3/2}\sigma^3 \int \phi_\mu \phi_\nu \phi_\gamma \phi_\delta \mathrm{d}\mathbf{r} \tag{8}$$

are normalized so that $K_{0000} = 1$, and they vanish for transitions that do not conserve parity. It should be noted that, when there is a cutoff in the sum over modes, both the regularized and non-regularized delta-function potential lead to the same Hamiltonian $\hat{H}$ and matrix elements in equation (8), and thus they produce the same results in the regularized (cutoff) quantum field theory. We emphasize that after the renormalization of the two-body interaction energy, the induced three-body interaction energy is insensitive to the cutoff Λ. We develop the perturbation theory in the small parameter ξ defined by

$$\xi \equiv \frac{\tilde{U}_2}{\hbar\omega} = \sqrt{\frac{2}{\pi}}\frac{a_{\mathrm{scat}}}{\sigma} + \mathcal{O}(a_{\mathrm{scat}}^2). \tag{9}$$

The total interaction energy for n atoms in the vibrational ground state in the single mode per site approximation is $E_{\mathrm{int}} = \tilde{U}_2 n(n-1)/2$. Commonly, a single-mode approximation is made based on the two-body interaction energy *per particle* being much less than the band gap, i.e. $E_{\mathrm{int}}/n = \tilde{U}_2(n-1)/2 \ll \hbar\omega$ or $n\xi \ll 1$. For ^{87}Rb with scattering length $a_{\mathrm{scat}} \simeq 5.3\,\mathrm{nm}$ and a lattice with $\omega/2\pi \simeq 30\,\mathrm{kHz}$, we have $\tilde{U}_2/h \simeq 2.0\,\mathrm{kHz}$, and $\xi = 0.07$. We will use these as typical system parameters in the following analysis. With $\xi = 0.07$, the single mode per site condition $n \ll \xi^{-1} \sim 15$ is easily satisfied and the influence of higher bands will produce only small (though important) corrections. For coherent states, for example, we show that small three-body energies can lead to large phase shifts over time resulting in interferometric-like sensitivity to higher-body and higher-band processes.

To obtain an effective Hamiltonian $\tilde{H}_{\mathrm{eff}}$, we use the multi-mode Hamiltonian $\hat{H} = \hat{H}_0 + \hat{H}_2$ to compute the atom-number-dependent energy shift for atoms in the vibrational ground state. Our approach is essentially equivalent to the effective field theory procedure of summing up to a cutoff over all 'high-energy' modes μ with $E_\mu \geqslant \hbar\omega$, which generates a low-energy effective theory with all consistent local interactions. We obtain an effective Hamiltonian $\tilde{H}_{\mathrm{eff}}$ for the

$\mu = 0$ mode that is valid in the low-energy regime $E_{\rm int}/n \sim n\tilde{U}_2 \ll \hbar\omega$, which is consistent with the single mode approximation discussed above. Of course the multimode Hamiltonian $\hat{H}$ itself is an effective Hamiltonian which is only valid for energy scales $E_\mu + E_{\rm int}/n \ll \hbar/(m_a a_{\rm scat}^2)$.

In the case of atoms confined in a deep well, the effective Hamiltonian for $\tilde{U}_2 \ll \hbar\omega$ is

$$\tilde{H}_{\rm eff} = E_0 \hat{a}^\dagger \hat{a} + \sum_{m>1} \tilde{U}_m \hat{a}^{\dagger m} \hat{a}^m / m!, \tag{10}$$

where $\hat{a}^\dagger$ creates an atom in a renormalized ground vibrational state. The $E_0 \hat{a}^\dagger \hat{a}$ term vanishes since we set $E_0 = 0$. The dominant term in $\tilde{H}_{\rm eff}$ is the two-body energy, and the higher-body interaction energies scale as $n\tilde{U}_m/\tilde{U}_{m-1} \sim (n\tilde{U}_2/\hbar\omega) \sim n\xi \ll 1$.

The energies $\tilde{U}_m$ can be computed in perturbation theory in the small parameter ξ using $\hat{H}$ to find the energy of n atoms in the ground vibrational mode. At mth order in ξ, all local interactions up through the $(m+1)$-body term $\tilde{H}_{m+1} = \tilde{U}_{m+1} \hat{a}^{\dagger m+1} \hat{a}^{m+1}/(m+1)!$ are generated. In this paper, we work to second order in ξ for which the effective Hamiltonian is

$$\tilde{H}_{\rm eff} = \tilde{U}_2 \hat{a}^{\dagger 2} \hat{a}^2/2 + \tilde{U}_3 \hat{a}^{\dagger 3} \hat{a}^3/6. \tag{11}$$

Using $\hat{n} = \hat{a}^\dagger \hat{a}$ and $[\hat{a}, \hat{a}^\dagger] = 1$, the two- and three-body terms can be written as $\hat{a}^{\dagger 2} \hat{a}^2 = \hat{n}(\hat{n}-1)$ and $\hat{a}^{\dagger 3} \hat{a}^3 = \hat{n}(\hat{n}-1)(\hat{n}-2)$; the latter expression shows explicitly that the effective three-body interaction only arises when there are three or more atoms in a well. Eigenstates of $\tilde{H}_{\rm eff}$ with n atoms have energies

$$\tilde{E}(n) = \tilde{U}_2 n(n-1)/2 + \tilde{U}_3 n(n-1)(n-2)/6. \tag{12}$$

Note that the three-body energy scales as n^3 and thus its influence relative to the two-body term, though small, can be tuned by changing the number of atoms in a well.

3. Mechanism for effective interactions

We now describe the virtual processes that give rise to effective m-body interactions in a deep lattice. Writing the perturbative expansion for the energy of an n atom state $|n\rangle$ through second order as $\tilde{E}(n) = E^{(0)}(n) + E^{(1)}(n) + E^{(2)}(n)$, the zeroth-order energy is $E^{(0)}(n) = E_0 n = 0$, recalling that $E_0 = 0$. The first-order energy shift, treating $\hat{H}_2$ as the perturbation Hamiltonian, is the usual expression

$$E^{(1)}(n) = \langle n|\hat{H}_2|n\rangle = \tilde{U}_2 n(n-1)/2. \tag{13}$$

This is the leading order result for the two-body interaction energy and, setting $n = 2$, the renormalization condition equation (7) shows that $A = 0$ to first order in $\tilde{U}_2$. Figure 1(a) represents this first-order process.

The second-order energy shift can be written as

$$E^{(2)}(n) = -\frac{\tilde{U}_2^2}{4} \sum_{\mu \geqslant \nu}^{\Lambda} \frac{s_{\mu\nu} K_{\mu\nu}^2 \left| \langle \mu\nu | \, \hat{a}_\mu^\dagger \hat{a}_\nu^\dagger \hat{a}_0 \hat{a}_0 \, |n\rangle \right|^2}{E_{\mu\nu}} + An(n-1)/2 \tag{14}$$

with $K_{\mu\nu} \equiv K_{\mu\nu 00}$ and $\mu \geqslant \nu$. The $\mathcal{O}(\tilde{U}_2^2)$ counter-term A now appears. At this order, A is determined by the renormalization condition $\tilde{E}(2) = E^{(0)}(2) + E^{(1)}(2) + E^{(2)}(2) = \tilde{U}_2$, implying that $E^{(2)}(2) = 0$. The sum is over intermediate states $|\mu\nu\rangle \equiv \hat{a}_\mu^\dagger \hat{a}_\nu^\dagger \hat{a}_0 \hat{a}_0 \, |n\rangle$ with energy $E_{\mu\nu} = E_\mu + E_\nu > 0$; this excludes the $\mu = \nu = 0$ state. For regularization purposes we introduce a high-energy cutoff that limits the sum to $E_{\mu\nu} \leqslant \Lambda$. The factor $s_{\mu\nu} = \{4, 1\}$ if $\{\mu = \nu, \mu \neq \nu\}$ comes

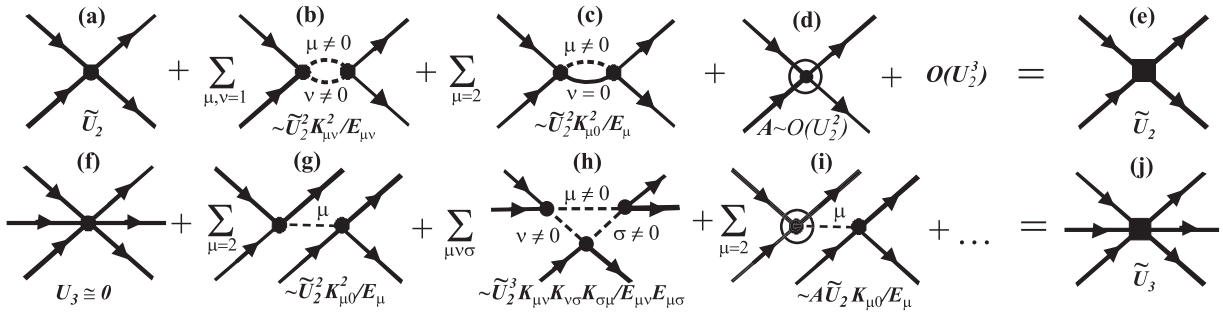

Figure 1. The effective two-body interaction energy $\tilde{U}_2$ is given through second order by diagrams (a)–(d). Diagram (d) is the counter-term that cancels the diagrams (b) and (c), fixing $\tilde{U}_2$ as the physical (renormalized) two-body energy. Diagrams (f)–(i) are examples of processes contributing to the effective three-body interaction energy $\tilde{U}_3$, represented by diagram (j). Diagram (g) gives the leading order contribution, assuming $U_3 = 0$; it shows how an effective three-body interaction involving three distinct incoming particles arises at second order in perturbation theory. Diagrams (h) and (i) are two of the effective three-body processes that arise at third order (others are not shown). If the bare three-body vertex shown in (f) does not vanish additional three (and higher) body counter-terms are also required.

from the two equivalent terms $\hat{a}_\mu^\dagger \hat{a}_\nu^\dagger$ and $a_\nu^\dagger \hat{a}_\mu^\dagger$ that appear in $\hat{H}_2$. Each term in $E^{(2)}$ involves a two-body collision-induced transition to a virtual intermediate state. For example, the state $|1_x 1_x\rangle$ corresponds to two atoms both excited along the x-direction with energy $E_{11} = 2\hbar\omega$ (note that $K_{11}^2 = 1/4$ for this transition), with the remaining $n-2$ atoms left in the $\mu = 0$ mode. Because collisions conserve parity, contributions from states like $|1_x 1_y\rangle$ vanish.

The crucial observation is that the series in equation (14) separates into two distinct sums corresponding to two-body and three-body interactions, respectively, i.e.

$$E^{(2)}(n) = \delta U_2 n(n-1)/2 + \delta U_3 n(n-1)(n-2)/6, \tag{15}$$

where δU_2 includes the counter-term contribution A from equation (14). For $\mu \neq 0$ *and* $\nu \neq 0$ intermediate states, $|\langle \mu\nu|\hat{a}_\mu^\dagger \hat{a}_\nu^\dagger \hat{a}_0 \hat{a}_0 |n\rangle|^2 = \kappa n(n-1)$ where $\kappa = \{2, 1\}$ if $\{\mu = \nu, \mu \neq \nu\}$, with the factor of 2 resulting from Bose stimulation when both atoms transition to the same excited state. Because these terms are proportional to $n(n-1)$ they contribute to the two-body energy shift δU_2. A diagram representing this two-body process, with two atoms colliding, making transitions to virtual excited vibrational states, and then returning to the ground state after a second collision with each other, is shown in figure 1(b). The $\mu \neq 0$ virtual states and $\mu = 0$ vibrational ground states are represented by dashed and solid lines, respectively.

The origin of the three-body energy can be seen by examining the $\mu > 0$, $\nu = 0$ intermediate states. We have

$$|\langle \mu\nu|\hat{a}_\mu^\dagger \hat{a}_0^\dagger \hat{a}_0 \hat{a}_0 |n\rangle|^2 = n(n-1)^2 = n(n-1) + n(n-1)(n-2), \tag{16}$$

showing that these terms generate both effective two- and three-body energies. The extra factor of $(n-1)$ in equation (16) results from Bose stimulation of an atom back into the $\mu = 0$ state when two atoms collide but only one makes a transition to an excited state. Figure 1(c) shows the two-body process corresponding to the $n(n-1)$ term in equation (16). Figure 1(d) shows the counter-term A whose value is determined such that it cancels the contributions

from figures 1(b) and (c), thereby maintaining, through second order, the renormalization condition that the parameter $\tilde{U}_2$ is equal to the physical two-body energy. To arbitrary order the renormalization condition determines A such that all higher-order two-body diagrams cancel, as represented by figure 1(e).

Figure 1(g) shows the effective three-body process corresponding to the $n(n-1)(n-2)$ term in equation (16). This process gives the leading-order contribution to δU_3 and generates a three-body interaction energy $\tilde{U}_3 = U_3 + \delta U_3$ even if the bare U_3, represented by figure 1(f), vanishes. More generally, we expect $U_3 \neq 0$, but nevertheless the contribution to $\tilde{U}_3$ given by δU_3 can be a significant (possibly even dominant) correction. Looking at figure 1(g), we see that two initial $\mu = 0$ atoms collide giving rise to one $\mu \neq 0$ atom that subsequently collides with a *third*, distinct $\mu = 0$ atom. In figure 1(g) there are three distinct incoming atoms resulting in an effective three-body interaction mediated by the $\mu \neq 0$ intermediate state. The renormalized three-body interaction energy is represented in figure 1(j) by a square vertex with three incoming and outgoing particles. Figures 1(h) and (i) show examples of two different processes contributing to $\tilde{U}_3$ at third order in ξ; they illustrate how higher-order processes, including counter-terms, arise. Their contributions, and other third-order processes not shown, are not explicitly computed below. At third order, effective four-body interactions also arise.

Note that there are two types of diagrams in figure 1: tree diagrams (e.g. figure 1(g)) and loop diagrams (e.g. figure 1(b)). In general in quantum field theory the contributions from some loop diagrams diverge with the cutoff Λ, necessitating the need for renormalization, whereas the contributions from tree diagrams are finite [30]. We will see this behavior explicitly below. In fact, at mth order in ξ, there will be a set of tree diagrams giving a *finite*, leading-order contribution to the effective $(m+1)$-body interaction energies $\tilde{U}_{m+1}$. We note that even if all intrinsic higher-body interactions exactly vanish there will be effective m-body interactions and associated energy scales $\tilde{U}_m$ generated by the two-body interactions. Consequently, the non-equilibrium dynamics of n atoms in the ground vibrational mode, when $n\xi \ll 1$, will be characterized by a hierarchy of frequencies $(\tilde{U}_2/h, \tilde{U}_3/h, \ldots, \tilde{U}_m/h)$.

4. Estimate of the effective three-body interaction energy

Returning to equation (14) for the second-order energy shift and separating it into two- and three-body parts, we find that

$$\delta U_2 = -\tilde{U}_2^2 \left(\sum_{\mu,\nu}^{\Lambda} K_{\mu\nu}^2 / E_{\mu\nu} \right) + A, \tag{17}$$

and

$$\delta U_3 = -6\tilde{U}_2^2 \left(\sum_{\mu>0}^{\Lambda} K_{\mu 0}^2 / E_{\mu 0} \right). \tag{18}$$

In the expression for δU_2 the sum is over all μ and ν (both $\mu > \nu$ and $\nu > \mu$) except for the $\mu = \nu = 0$ mode. Similarly, in the expression for δU_3 all μ except for $\mu = 0$ are summed over.

As expected, the sum $\sum_{\mu,\nu}^{\Lambda} K_{\mu\nu}^2/E_{\mu\nu}$ corresponding to the second-order, 1-loop diagram in figure 1(b) diverges with Λ, reflecting the divergent relationship between the bare U_2 and renormalized $\tilde{U}_2$ energy parameters. In fact, the sum scales with the cutoff as $\Lambda^{1/2}$. The renormalization condition that $\tilde{E}(2) = \tilde{U}_2$ determines A by requiring that $\delta U_2 = 0$. To

second-order, the interaction energy of n atoms is thus

$$\tilde{E}(n) = \tilde{U}_2 n(n-1)/2 + \delta U_3 n(n-1)(n-2)/6, \tag{19}$$

assuming $\tilde{U}_3 = \delta U_3$.

After canceling the two-body corrections with A, the remaining second-order term gives an induced three-body energy that is insensitive to Λ: the quantity $\sum_{\mu>0}^{\Lambda} K_{\mu 0}^2/E_{\mu 0}$ corresponding to the second-order tree diagram in figure 1(g) converges. Writing

$$\delta U_3/\hbar\omega = -\beta\xi^2, \tag{20}$$

this sum can be solved analytically for a spherically symmetric harmonic trap in the $\Lambda \to \infty$ limit, and we find[6]

$$\beta = 4\sqrt{3} - 6 + 6\log\left(\frac{4}{2+\sqrt{3}}\right) \simeq 1.34\ldots. \tag{21}$$

Cutting off the sum at $E_{\mu\nu}/\hbar\omega \leqslant \Lambda/\hbar\omega = 4$ already gives $\beta \simeq 1.30$ showing the rapid convergence of the series. The convergence of this sum is an example of the generic behavior that contributions from tree diagrams are finite. If the bare U_3 is zero or sufficiently small, the effective three-body energy is negative, giving attractive three-body interactions, and reducing the total interaction energy for both positive or negative $\tilde{U}_2$.

We expect significant corrections due to the anharmonicity of the true lattice potential. The single-particle energies of higher vibrational states are lowered on the order of the recoil energy E_{R}, defined as the gain in kinetic energy for an atom at rest that emits a lattice photon. This leads to a decrease of the energy denominator in equation (14) and, for the typical system parameters considered here, this can give an estimated correction to $\tilde{U}_3$ of 10% or more. The matrix elements $K_{\mu\nu}$ will also have corrections. These effects can be computed numerically using single-particle band theory.

We have defined our perturbation theory around the zero-collisional energy limit, but in a trap the collision energy of ground state atoms is of the order of $\hbar\omega$. As shown in [36], an improved treatment replaces the zero-energy scattering length by an effective scattering length defined as

$$-\frac{1}{a_{\mathrm{eff}}} = -\frac{1}{a_{\mathrm{scat}}} + \frac{1}{2} r_e k^2, \tag{22}$$

where the effective range r_{e} is of the order of the van der Waals length scale $\left(m_a C_6/\hbar^2\right)^{1/4}$ away from a Feshbach resonance, and the collision energy is $\hbar^2 k^2/m_a$ [37]. For ^{87}Rb the van der Waals length is approximately 8 nm. In a trap the ground vibrational state wavevector $k \simeq \sigma^{-1}$ produces a fractional increase in scattering length of the order of $(r_{\mathrm{e}}/\sigma)\xi$. By incorporating the effective scattering length model we can extend the range of validity of our model.

Even neglecting these corrections, the perturbation theory generated by equations (2) and (6) does not predict the two-body energy $\tilde{U}_2$ but instead uses the measured value, or the exact result calculated by other methods such as Busch *et al* [32], as input from which δU_3 is obtained. Similarly, the effective theory does not yield the intrinsic three-body interaction energy U_3, and therefore $\tilde{U}_3 = U_3 + \delta U_3$ must also be determined by either measurement or a

[6] An analytic expression for $K_{\mu 0}$ can be obtained by expressing $K_{\mu 0}$ as an integral over a generalized Laguerre polynomial, and then using an integral representation for the Laguerre polynomial. The sum in δU_3 can then be solved exactly with $\Lambda \to \infty$.

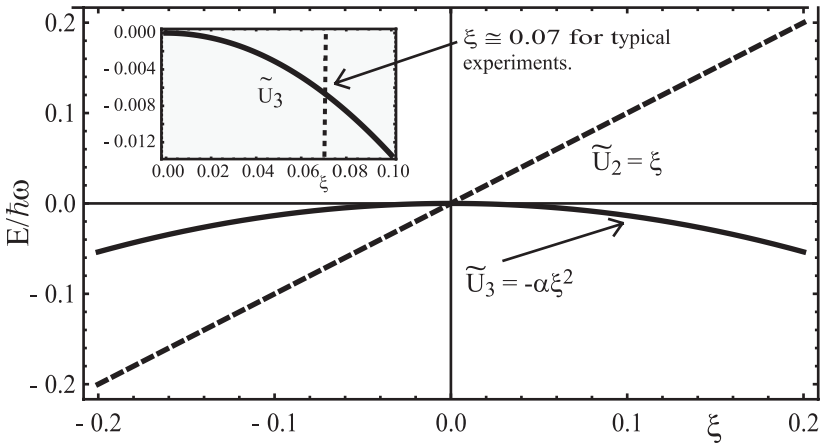

Figure 2. The figure shows $\tilde{U}_3$ and $\tilde{U}_2$, in units of $\hbar\omega$, versus ξ. The bold line shows the induced three-body energy $\delta\tilde{U}_3 = \tilde{U}_3 = -\beta\xi^2$ with $\beta = 1.34$, assuming the intrinsic energy U_3 vanishes. The dashed line shows the leading-order two-body energy $\tilde{U}_2$. The graphs extend beyond the regime of strict validity of the perturbation theory, which requires $\xi n \ll 1$, where n is the number of atoms in a lattice well, to illustrate the overall scaling of the two- and three-body energies. The collapse and revival experiments in [5]–[7] have $\omega/2\pi \sim 30\,\mathrm{kHz}$ and $\xi \sim 0.07$, putting them well within the perturbative regime. The inset shows $\tilde{U}_3$ for the range $0 < \xi < 0.1$.

theory of three-body physics if the intrinsic interaction energies $U_{m>2}$ are nonzero. On the other hand, the effective theory shows that even if $U_{m>2} = 0$ there are significant induced three- and higher-body interactions, and if nonzero $\tilde{U}_{m>2}$ are measured the effective contribution from two-body processes must be taken into account before the intrinsic higher-body coupling strengths can be extracted. Note that if nonzero bare (intrinsic) parameters $U_{m>2}$ are included in our model, additional counter-terms will be needed to cancel divergences, reflecting the need to ultimately determine any intrinsic higher-body coupling strengths via either measurement or an exact high-energy theory.

Assuming $U_3 \simeq 0$, figure 2 shows $\tilde{U}_2 = \xi\hbar\omega$ and $\tilde{U}_3$ versus ξ, including positive ($\xi > 0$) and negative ($\xi < 0$) scattering lengths. Using $\xi = 0.07$ for ^{87}Rb in a 30 kHz well gives $\tilde{U}_2/h \simeq 1.9\,\mathrm{kHz}$ and $\tilde{U}_3/h \simeq -200\,\mathrm{Hz}$. Using a Feshbach resonance [38] to change a_{scat} and thus ξ, or fixing a_{scat} and changing the trap frequency ω, it is possible to tune the relative strengths of the three-body (and higher-body) interactions. It would be interesting to explore the breakdown of the perturbative model by increasing either ξ or the atom number n, or by decreasing the lattice depth so that the influence of tunneling and higher-band effects increases.

5. Dynamics and decoherence of atom-number coherent states

We now investigate the influence of effective three-body interactions on the phase coherence of an N atom non-equilibrium state $|\Psi(0)\rangle = (\sum_{i=1}^{M} \hat{a}_{i0}^{\dagger}|0\rangle/\sqrt{M})^{\otimes N}$, obtained by quickly loading a BEC into a lattice with M sites. To a good approximation the state can be treated as the product of coherent states [5, 10],

$$|\Psi(0)\rangle \simeq \prod_i \exp(\sqrt{\bar{n}_i}\hat{a}_i^{\dagger})|0\rangle \simeq \prod_i |\alpha_i\rangle, \tag{23}$$

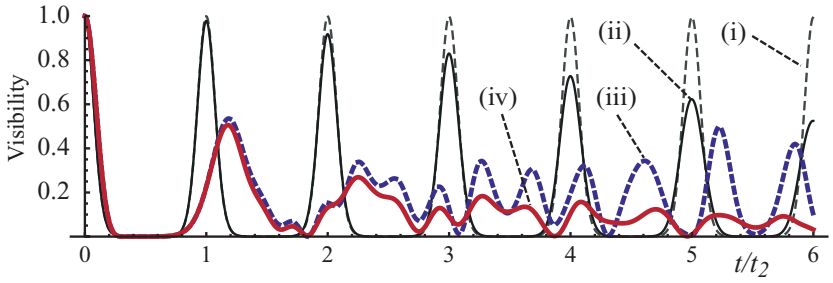

Figure 3. Collapse and revival visibility versus time t, with $\xi = 0.07$ and $\bar{n} = 2.5$. Curve (i) shows the case with neither inhomogeneities nor three-body interactions included. Curve (ii) shows the effects of ∼5% inhomogeneities in U_2. Curve (iii) shows the effects of three-body interactions with $\alpha = 1.34$ but no inhomogeneities. Note that the three-body mechanism influences the visibility of revivals immediately, and it will be important even if inhomogeneities are stronger than are shown in curve (ii). Curve (iv) shows the combined effects of inhomogeneities and three-body interactions.

where $\hat{a}_i|\alpha_i\rangle = \alpha_i|\alpha_i\rangle$ and $|\alpha_i|^2 = \bar{n}_i$ is the average number of atoms in the ith site. A relative phase ϕ_{ij} between sites $i \neq j$ exists when $\langle \hat{a}_i^\dagger \hat{a}_j \rangle = \eta e^{i\phi_{ij}}$ and $\eta \neq 0$. The initial state $|\Psi(0)\rangle$ has $\eta = \bar{n}$, and there are well-defined relative phases ($\phi_{ij} = 0$ for all i, j in this case). In contrast, the equilibrium Mott insulator state, achieved by much slower loading [34, 35], has approximate number states in each well giving $\eta \approx 0$, though there can be some degree of short-range phase coherence [39]–[41].

Coherent states in optical lattices make natural probes of higher-body coherent dynamics because small atom-number-dependent energies can lead to significant phase shifts over time. After a hold time t_h in the lattice, the initial state evolves to $|\Psi(t_h)\rangle \simeq \prod_i |\eta(t_h)\rangle_i$, where the state of the ith well is

$$|\eta\,(t_h)\rangle_i = e^{-\bar{n}_i/2} \sum_n \frac{\alpha_i^n}{\sqrt{n!}} |n\rangle_i \, e^{-i\tilde{E}_i(n)t_h/\hbar}, \tag{24}$$

and $\tilde{E}_i(n_i)$ is given in equation (12), restoring the index i labeling the lattice site. Snapping the lattice off at time t_h, the wavefunctions from each well freely expand for a time t_e until they fully overlap, analogous to the diffraction of light through a many-slit grating.

For a uniform lattice, the fringe visibility is [5]

$$V(t_h) = \left|\langle \eta\,(t_h)|\,\hat{a}\,|\eta\,(t_h)\rangle\right|^2/\bar{n}. \tag{25}$$

With no inhomogeneities and setting $\tilde{U}_3 = 0$, we obtain $V(t_h) = e^{-2\bar{n}[1-\cos(\tilde{U}_2 t_h/\hbar)]}$. The visibility for $\bar{n} = 2.5$ is plotted as the thin dashed line labeled (i) in figure 3, showing the well-known collapse and revival dynamics with period $t_2 = h/\tilde{U}_2$. For the ^{87}Rb system parameters used here $t_2 = 0.52$ ms.

The thin line labeled (ii) in figure 3 shows the influence of a ∼5% variation in the two-body energy U_2. We average the $a_i(t)$ over a 60 lattice-site diameter spherical distribution. While the effect of inhomogeneities are important, a larger variation in U_2 then expected would be required to explain the decay of interference fringes after only five revivals as seen in experiments [5]–[7]. We note that the longer timescale for three-body recombination can

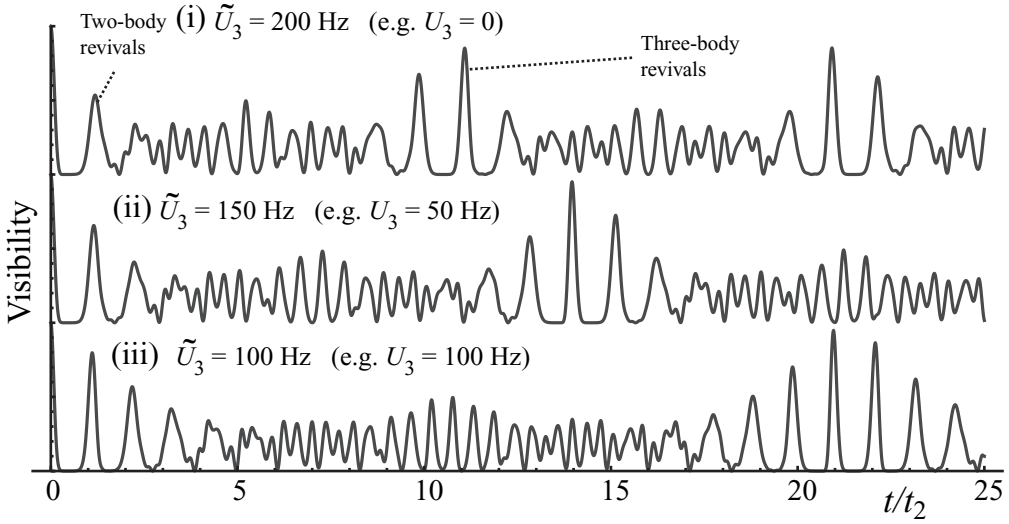

Figure 4. The figure shows the collapse and revival visibility versus time for $\tilde{U}_3 = 200$, 150 and 50 Hz assuming negligible inhomogeneities. Curve (i) corresponds to $U_3 = 0$, $\xi = 0.07$, $\alpha = 1.34$, $\bar{n} = 2.5$ and $\omega/2\pi = 30$ kHz. Curves (ii) and (iii) correspond to smaller three-body energies $\tilde{U}_3$, which could be due to a nonzero intrinsic U_3, a reduction in α, or a change in other system parameters including ξ or $\bar{n}$. Three-body revivals occur at multiples of $t_3 = h/\tilde{U}_3$, providing a method for measuring the coherent three-body interaction energy.

be distinguished from the coherent, number conserving interactions derived here by tracking changes in total atom number, and this appears to be negligible on the revival damping timescale [26]. Other mechanisms, such as non-adiabatic loading [42, 43] and collisions during expansion [44] will reduce the initial fringe visibility but do not explain the rapid decay of the visibility versus hold time $t_{\rm h}$.

To compute the visibility with three-body interactions we numerically evaluate

$$\langle \eta\,(t_{\rm h})|\,\hat{a}\,|\eta\,(t_{\rm h})\rangle = \alpha {\rm e}^{-\bar{n}} \sum_{n=0} \frac{\bar{n}^n}{n!} {\rm e}^{-in\left[\tilde{U}_2+\tilde{U}_3(n-1)/2\right]t_{\rm h}/\hbar}. \tag{26}$$

The bold (blue) dashed line labeled (iii) in figure 3 shows the visibility $V(t_{\rm h}) = |\langle\eta(t_{\rm h})|\hat{a}|\eta(t_{\rm h})\rangle|^2/\bar{n}$ versus $t_h/{\rm t}_2$ assuming no inhomogeneities, $\bar{n} = 2.5$, and the harmonic oscillator value $\beta = 1.34\ldots$. With $\xi = 0.07$, $U_3 = 0$, and $\omega/2\pi = 30$ kHz, the effective three-body frequency is $\tilde{U}_3/h \simeq -200$ Hz, and $\tilde{U}_2/h \simeq 2.1$ kHz. The relatively small effective three-body interactions have a strong effect on the coherence of the state and the resulting quantum interference, showing how collapse and revival measurements can be a sensitive probe of coherent higher-body effects. The dephasing is faster than may have been expected from the small size of $\tilde{U}_3$ because the three-body energies scale as $\tilde{U}_3 n^3$ versus $\tilde{U}_2 n^2$ for two-body energies, and thus have an increased influence on higher-number components of a coherent state. Similarly, coherent states with significant $n > 4$ atom number components will probe the four- and higher-body interaction energies. The bold (red) solid line labeled (iv) in figure 3 shows the combined effect of both ~5% inhomogeneities in $\tilde{U}_2$ and three-body interactions.

The decay of the visibility in figure 3 is faster than what is seen in [5]–[7]. Figure 4 illustrates the sensitivity of the evolution of the visibility to the three-body energy scale by

showing three cases corresponding to $\tilde{U}_3/h = \{-200, -150, -100\}$ Hz. The curves have been displaced vertically for clarity. Curve (i) for $\tilde{U}_3/h = -200$ Hz corresponds to $U_3 = 0$, $\beta = 1.34$, $\xi = 0.07$ and $\omega/2\pi = 30$ kHz. Curve (ii) corresponds to a reduced $\tilde{U}_3/h = -150$ Hz, which could be the result, for example, of a positive intrinsic three-body energy $U_3/h = 50$ kHz, or a change in parameters giving either $\beta \to 3\alpha/4$ or $\xi \to \sqrt{3}\xi/2$. Similarly, curve (iii) corresponds to $\tilde{U}_3 = 100$ Hz, which could be due to a positive intrinsic three-body energy $U_3/h = 100$ kHz, or to a change in parameters giving either $\beta \to \beta/2$ or $\xi \to \xi/\sqrt{2}$. The collapse and revival visibilities are also very sensitive to the average atom number $\bar{n}$. A smaller value of $\tilde{U}_3$ appears to agree better with the initial damping seen in [5]–[7], and this may indicate the presence of a nonzero intrinsic U_3. However, accurate measurement of the system parameters is necessary if a value of the intrinsic U_3 is to be obtained using $U_3 = \tilde{U}_3 - \delta U_3$. Nevertheless, it is clear from figure 4 that both intrinsic and induced three-body interactions can be important on experimentally relevant timescales.

Figure 4 also shows the partial and full revivals resulting from the beating between two- and three-body frequency scales expected if inhomogeneities are sufficiently reduced. The period for nearly full three-body revivals $t_3 = h/\tilde{U}_3$ gives a direct method of measuring $\tilde{U}_3$. Recently, long sequences of collapse and revivals showing multiple frequencies have been reported [26]; our analysis suggests that these may be used to study higher-body interactions in optical lattices.

6. Summary

We have shown that two-body induced virtual excitations of bosons to higher bands in a deep 3D optical lattice generate effective three-body and higher-body interactions. Although our methods do not yield the intrinsic higher-body interaction energies U_m, we find that even if $U_m \simeq 0$ there are significant effective interactions that can have a surprisingly strong influence on the dynamics of non-equilibrium coherent states. The mechanism for higher-body interactions is based upon the recognition that at low energies the presence of excited (i.e. higher-energy) vibrational states manifest as m-body terms in an effective Hamiltonian $\tilde{H}_{\text{eff}}$. While it is possible for an effective (or renormalized) m-body interaction to vanish or to be very small due to close cancellation of the intrinsic (i.e. U_m) and induced (i.e. δU_m) contributions to $\tilde{U}_m$, we do not expect this to happen in general. It is possible to tune the relative effective m-body interactions by exploiting Feshbach resonances to control a_{scat}, or by changing the lattice potential. This suggests intriguing possibilities for probing and controlling the physics of effective field theories (e.g. effective interactions, running coupling constants and the emergence of non-perturbative effects) in optical lattices. Using optical lattices to simulate the controlled breakdown of an effective field theory would be particularly interesting.

Acknowledgments

We thank J Sebby-Strabley and W D Phillips for very helpful conversations. PRJ acknowledges support from the Research Corporation for Science Advancement. JVP acknowledges support from IARPA.

References

[1] Wright E M, Walls D F and Garrison J C 1996 *Phys. Rev. Lett.* **77** 2158
[2] Wright E M, Wong T, Collett M J, Tan S M and Walls D F 1997 *Phys. Rev.* A **56** 591

[3] Milburn G J, Corney J, Wright E M and Walls D F 1997 *Phys. Rev.* A **55** 4318
[4] Walls D F, Collett M J, Wong T, Tan S M and Wright E M 1997 *Phil. Trans. R. Soc.* A **355** 2393
[5] Greiner M, Mandel O, Hänsch T W and Bloch I 2002 *Nature* **419** 51
[6] Anderlini M, Sebby-Strabley J, Kruse J, Porto J V and Phillips W D 2006 *J. Phys. B: At. Mol. Opt. Phys.* **39** S199–210
[7] Sebby-Strabley J, Brown B L, Anderlini M, Lee P J, Johnson P R, Phillips W D and Porto J V 2007 *Phys. Rev. Lett.* **98** 200405
[8] Pethick C J and Smith H 2002 *Bose–Einstein Condensation in Dilute Gases* (Cambridge: Cambridge University Press)
[9] Haroche S and Raimond J-M 2006 *Exploring the Quantum* (Oxford: Oxford University Press)
[10] Bloch I, Dalibard J and Zwerger W 2008 *Rev. Mod. Phys.* **80** 885
Bloch I 2008 *Nature* **453** 1016
[11] Efimov V N 1970 *Phys. Lett.* B **33** 563
[12] Bedaque P F, Braaten E and Hammer H-W 2000 *Phys. Rev. Lett.* **85** 908
[13] Kraemer T *et al* 2006 *Nature* **440** 315–8
[14] Burt E A, Ghrist R W, Myatt C J, Holland M J, Cornell E A and Wieman C E 1997 *Phys. Rev. Lett.* **79** 337
[15] Esry B D, Greene C H and Burke J P 1999 *Phys. Rev. Lett.* **83** 1751
[16] Stoll M and Kohler T 2005 *Phys. Rev.* A **72** 022714
[17] Petrov D S 2005 *Phys. Rev.* A **71** 012708
[18] Braaten E and Hammer H-W 2006 *Phys. Rep.* **428** 259
[19] Ferlaino F, Knop S, Berninger N, Harm W, D'Incao J P, Nägerl H-C and Grimm R 2009 *Phys. Rev. Lett.* **102** 140401
[20] Huckans J H, Williams J R, Hazlett E L, Stites R W and O'Hara K M 2009 *Phys. Rev. Lett.* **102** 165302
[21] Chen B-L, Huang X-B, Kou S-P and Zhang Y 2008 *Phys. Rev.* A **78** 043603
[22] Schmidt K P, Dorier J and Läuchli A M 2008 *Phys. Rev. Lett.* **101** 150405
[23] Capogrosso-Sansone B, Wessel S, Büchler H P, Zoller P and Pupillo G 2009 *Phys. Rev.* B **79** 020503
[24] Lutchyn R M, Tewari S and Sarma S D 2009 *Phys. Rev.* A **79** 011606
[25] Micheli A, Zoller P and Büchler H P 2007 *Nat. Phys.* **3** 726
[26] Will S, Best T, Braun S, Schneider U, Hackermüller L, Lühmann D-S and Bloch I 2009 *Bull. Am. Phys. Soc.* **54** 121
[27] Fischer U R and Schützhold R 2008 *Phys. Rev.* A **78** 061603
[28] Fölling S, Trotsky S, Cheinet P, Feld N, Saers R, Widera A, Müller T and Bloch I 2007 *Nature* **448** 1029
[29] Ananikian D and Bergeman T 2006 *Phys. Rev.* A **73** 013604
[30] Srednicki M 2007 *Quantum Field Theory* (Cambridge: Cambridge University Press)
[31] Huang K and Yang C N 1957 *Phys. Rev.* **105** 767
[32] Busch T, Englert B-G, Rzążewski K and Wilkens M 1998 *Found. Phys.* **28** 549
[33] Fisher M P A, Weichman P B, Grinstein G and Fisher D S 1989 *Phys. Rev.* B **40** 546–70
[34] Jaksch D, Bruder C, Cirac J I, Gardiner C W and Zoller P 1998 *Phys. Rev. Lett.* **81** 3108
[35] Greiner M, Mandel O, Esslinger T, Hänsch T W and Bloch I 2002 *Nature* **415** 39
[36] Bolda E L, Tiesinga E and Julienne P S 2002 *Phys. Rev.* A **66** 013403
[37] Gao B 1998 *Phys. Rev.* A **58** 4222
[38] Tiesinga E, Verhaar B J and Stoof H T C 1993 *Phys. Rev.* A **47** 4114
[39] Gerbier F, Widera A, Fölling S, Mandel O, Gericke T and Bloch I 2005 *Phys. Rev. Lett.* **95** 050404
[40] Roberts D C and Burnett K 2003 *Phys. Rev. Lett.* **90** 150401
[41] Roth R and Burnett K 2003 *Phys. Rev.* A **67** 031602
[42] Hecker-Denschlag J, Simsarian J E, Häffner H, McKenzie C, Browaeys A, Cho D, Helmerson K, Rolston S and Phillips W D 2002 *J. Phys. B: At. Mol. Opt. Phys.* **35** 3095
[43] Rey A M, Pupillo G and Porto J V 2006 *Phys. Rev.* A **73** 023608
[44] Gerbier F *et al* 2008 *Phys. Rev. Lett.* **101** 155303